Available online at www.sciencedirect.com
ScienceDirect
Acta Materialia 59 (2011) 1651–1658
Acta MATERIALIA
www.elsevier.com/locate/actamat

Effects of solidification kinetics on microstructure formation in binary Sn–Cu solder alloys

Tina Ventura [a], Sofiane Terzi [a], Michel Rappaz [b], Arne K. Dahle [a,*]

[a] Materials Engineering, The University of Queensland, Brisbane, Queensland 4072, Australia
[b] Computational Materials Laboratory, Ecole Polytechnique Fédérale Lausanne, 1015 Lausanne, Switzerland

Received 4 August 2010; received in revised form 4 November 2010; accepted 12 November 2010
Available online 7 December 2010

Abstract

Three binary Sn–Cu solder alloys of near-eutectic composition have been directionally solidified at different growth rates. The competition between primary tetragonal Sn cells/dendrites and eutectic is interpreted with the coupled zone concept. It is also found that Sn–Cu is a weakly irregular eutectic system with Cu_6Sn_5 leading the eutectic, but two different eutectic morphologies (coarse and fine) form simultaneously during eutectic growth. At higher growth rates, the eutectic interface breaks down into a cellular eutectic with the fine eutectic in the centre of the cells and the coarse one at the cell boundaries. This is explained by the segregation of Pb impurities ahead of the eutectic interface.

Keywords: Solidification; Lead-free solder; Eutectic; Dendritic growth

1. Introduction

In the electronics industry traditional lead-based solders have been used for many years to effectively solder electronic circuit boards. These solders have many advantages in terms of behaviour and properties for soldering, in particular a low melting point ($T_m = 183$ °C for a eutectic Sn–Pb alloy), which makes them suitable for use in heat-sensitive electronic components. However, in recent years, legislation has specifically targeted the widespread use of lead because of its environmental impact (e.g. Restriction of Hazardous Substances Directive (RoHS) in the European Union [1]). The search for an optimum lead-free solder replacement with similar properties is ongoing.

For wave soldering applications, an attractive replacement solder is the near-eutectic Sn–0.7 wt.% Cu alloy [2]. This alloy has shown excellent solderability in commercial production and it also presents cost advantages compared to Ag-containing alternatives [2]. It has been shown that ppm level additions of Ni enhance the soldering properties of the Sn–0.7 wt.% Cu alloy by reducing the tendency for bridging and improving the solder–substrate interface and the surface finish [3,4]. Although nickel has a strong influence on solderability, the detailed mechanism is not fully understood. Even for the binary Sn–Cu system, there is very limited knowledge of the solidification kinetics, despite several investigations [5–8].

The purpose of the current research was to investigate the solidification of binary Sn–Cu solder alloys, and to get a better understanding of this system before investigating the influence of ternary additions. Directional solidification experiments in a Bridgman furnace were performed at various pulling rates for three binary near-eutectic Sn–Cu alloys with composition Sn–0.5 Cu, Sn–0.7 Cu and Sn–0.9 Cu (all compositions in wt.%). The microstructural observations are interpreted with the help of the phase diagrams proposed in the literature, taking into account the competition that exists between the primary phase and the eutectic (so-called "coupled zone" [9]).

* Corresponding author.
E-mail address: a.dahle@uq.edu.au (A.K. Dahle).

1359-6454/$36.00 © 2010 Acta Materialia Inc. Published by Elsevier Ltd. All rights reserved.
doi:10.1016/j.actamat.2010.11.032

2. Experimental method

Three binary Sn–Cu alloys, Sn–0.5 wt.% Cu, Sn–0.7 wt.% Cu and Sn–0.9 wt.% Cu, were prepared by mixing industrial solder ingots of Sn–0.7 wt.% Cu with pure Sn and Sn–10 wt.% Cu in clay–graphite crucibles and melting in an electric resistance furnace at a temperature of 350 °C. The mean chemical compositions of the alloys were confirmed by X-ray fluorescence (XRF) analysis and are reported in Table 1.

The specimens for the directional solidification (DS) experiments were produced by drawing the molten alloy into a Pyrex glass tube (inside diameter = 6 mm), which was then allowed to cool and solidify. The experiments were carried out in a classical Bridgman furnace. The samples were withdrawn at a given velocity (v) in a uni-directional temperature gradient (G) of about 2.5 K mm^{-1}. No indications of a radial gradient component were observed in any of the DS samples in this work. After 60 mm of growth, the specimens were dropped into cold water at 5 °C to quench the microstructure. Experiments were carried out with six different velocities from 2 to 100 μm s^{-1}. The thermal conditions were measured by mounting a K-type thermocouple inside the tube in contact with the molten metal.

After quench, the samples were sectioned with a band saw, mounted in epoxy resin and then ground using SiC papers (180–500 grit) and diamond suspensions (9, 6 and 3 μm). The final polishing step was performed in a mixture of 96% OPS (0.05 μm colloidal silica), 2% ammonium hydroxide and 2% hydrogen peroxide (30%) to slightly etch the Sn phase and improve the contrast for optical microscopy.

Optical micrographs of the steady-state growth morphology were taken with a Reichert Polyvar reflected light microscope using a Canon digital camera. A JEOL JSM-6460LA scanning electron microscope at 20 kV acceleration voltage was used for higher magnification characterisation.

For the image analysis, optical and scanning electron microscopy micrographs were binarized with reference to the grey level of the Sn matrix. The eutectic fibre spacing λ_E were determined from a Voronoi tessellation of the fibre centres and the fibre diameter d was calculated from the equivalent disk surface.

3. Results

The DS microstructures of the three binary alloys, Sn–0.5 Cu, Sn–0.7 Cu and Sn–0.9 Cu, solidified at various speeds, can be classified as fully eutectic (FE) or off-eutectic (OE). The first type corresponds to the coupled growth of Cu_6Sn_5 rods or fibres in a β-Sn matrix, whereas the second exhibits primary β-Sn cells or dendrites surrounded by eutectic. Fig. 1 shows longitudinal (top) and transverse (bottom) cross-sections of the three alloys grown at the same speed, 10 μm s^{-1}.

In the Sn–0.5 Cu specimen (Fig. 1a), primary β-Sn dendrites are clearly visible: in the transverse section (bottom) the trunks are arranged in layers separated by a spacing on the order of 300 μm. These dendrites are surrounded by a fine eutectic structure growing with a nearly planar front morphology, about 0.5 mm behind the quenched dendrite tips (Fig. 1a, top).

Increasing the Cu content to 0.7 wt.% (Fig. 1b) leads to a more cellular primary phase morphology with almost no side branches. The distance between the cell tips and the eutectic front has been reduced compared to the previous specimen and the trunks are no longer aligned along a direction in the transverse section. At 0.9 wt.% Cu (Fig. 1c), the microstructure does not contain any more primary β-Sn phase cells or dendrites and is made of a fine eutectic, with Cu_6Sn_5 fibres surrounded by the β-Sn matrix. The eutectic front at this magnification appears nearly flat.

Now changing the velocity at which the DS specimens were solidified, the various morphologies that were obtained are summarized in Fig. 2, with open circles for FE microstructures and filled triangles and diamonds for OE microstructures with cellular and dendritic primary phase, respectively. Cellular eutectic (CE) structures, which will be described in more detail later, are represented with open squares. The transition between FE and OE or CE structures occurs at increasing speed with increasing Cu concentration.

For OE microstructures observed in the Sn–0.5 Cu and Sn–0.7 Cu specimens, the primary spacing between successive rows of primary trunks (see Fig. 1a, bottom) has been measured and corresponds to a primary trunk spacing, λ_1. In the case of OE primary phase cells (Fig. 1b, bottom), the λ_1 spacing has been determined as the inverse square root of the density of primary cells observed in a transverse cross-section. On the other hand, the spacing between dendrite or cell tips and the eutectic interface has been converted into a temperature difference or freezing range, ΔT, using the measured temperature gradient (2.5 K mm^{-1}) (see Fig. 3a). The observations made for these two alloys solidified at various speeds, namely the primary trunk spacing λ_1, the freezing range ΔT and the type of primary phase (cells/dendrites) are summarized in Table 2.

Table 1
Compositions of the alloys studied in this work measured by XRF analysis (wt.%).

Sample	Sn	Cu	Ni	Pb	Ag	Sb	Bi	Zn	Fe	Al	As	Cd
Sn0.5 Cu	Bal.	0.513	0.004	0.035	0.006	0.020	0.006	<0.001	0.004	<0.001	0.006	<0.001
Sn0.7 Cu	Bal.	0.700	0.009	0.030	0.009	0.014	0.027	<0.001	0.005	<0.001	<0.001	<0.001
Sn0.9 Cu	Bal.	0.919	0.006	0.036	0.005	0.021	0.008	<0.001	0.004	<0.001	0.008	<0.001

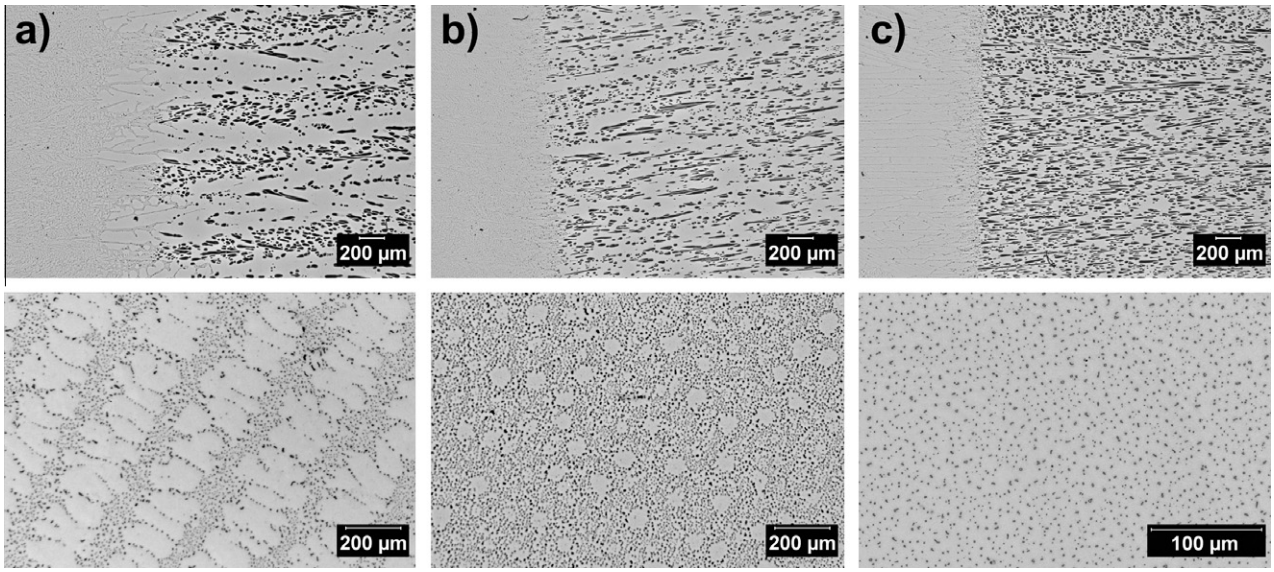

Fig. 1. Longitudinal (top) and transverse (bottom) cross-sections of Bridgman samples solidified at 10 μm s^{-1}. (a) OE structure with primary dendrites followed by a eutectic interface (Sn–0.5 Cu), (b) OE structure with primary cells followed by a eutectic interface (Sn–0.7 Cu) and (c) FE structure with random distribution of Cu_6Sn_5 fibres (Sn–0.9 Cu).

As can be seen in Table 2, the primary spacing of dendrites, λ_1, decreases with increasing growth rate, but without any significant effect of the Cu content. However, the λ_1 spacing measured for cellular primary morphology is substantially smaller. The freezing range ΔT first increases with increasing velocity and then becomes nearly constant for both alloys (1.8 K for Sn–0.5 Cu and 0.5 K for Sn–0.7 Cu). For Sn–0.7 Cu solidified at 20 μm s^{-1}, ΔT could not be measured due to the sample breaking at the solid/liquid interface during quench. The nearly constant freezing ranges of these two alloys are smaller than the equilibrium values deduced from the difference between the corresponding liquidus and eutectic temperatures (2.2 K and 1 K, respectively) [10,11].

Focusing now on the eutectic morphology, the nearly-planar eutectic front at low magnification is not strictly isothermal at higher magnification (see Fig. 3b): the interface consists of leading Cu_6Sn_5 fibres or rods surrounded by the Sn matrix. However, the distance over which the eutectic front spreads is small, typically on the order of 50 μm (i.e., 0.12 K difference). This is characteristic of a weakly irregular eutectic, with not too much branching difficulties of the faceted phase (in this case the Cu_6Sn_5 fibres) [12].

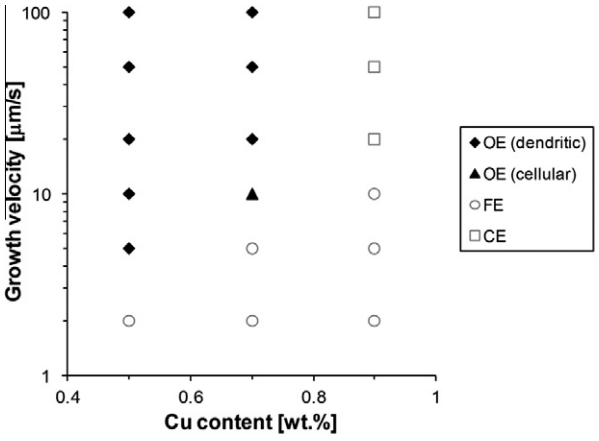

Fig. 2. Solidification microstructure types observed in Sn–Cu alloys recorded as a function of alloy composition and growth velocity.

The eutectic morphology of FE Sn–0.9 Cu specimens is not uniform and can be either fine or coarse. This is shown in Fig. 4a for a Sn–0.9 Cu specimen solidified at 2 μm s^{-1}. The figure shows the boundary between two eutectic "grains" or domains, one with a very fine fibre spacing and the other with a much coarser morphology and larger spacing. This is surprising for steady-state growth at the same velocity of a unique composition specimen. Even more surprising, each type of morphology can be found in all the Sn–0.9 Cu specimens solidified at low speed (2–10 μm s^{-1} – FE structures, Fig. 2), and each of them follows a typical $\lambda_E^2 v = \text{constant}$, as shown in Fig. 5a. The twofold difference in the λ_E spacing of the two eutectic morphologies translates into a fourfold difference in the $\lambda_E^2 v$ scale used on the vertical axis of this diagram, whereas the horizontal axis corresponds to the inverse of the velocity. As can be seen, each morphology follows a least squares linear fit. In order to keep the phase fraction nearly constant, the diameter d of the fibres also scales with $d^2 v = \text{constant}$, as shown in Fig. 5b. Similar cellular or double-type eutectic structures are observed for the two other compositions, as shown in Fig. 4b for a Sn–0.7 Cu specimen solidified at 20 μm s^{-1}.

The intermetallic area fraction, measured in cross-sections by a surface pixel count for the three alloys solidified with a FE morphology, is shown in Fig. 6 for the various velocities. For all three alloys the area fractions are shown separately for the coarse and fine eutectic microstructures.

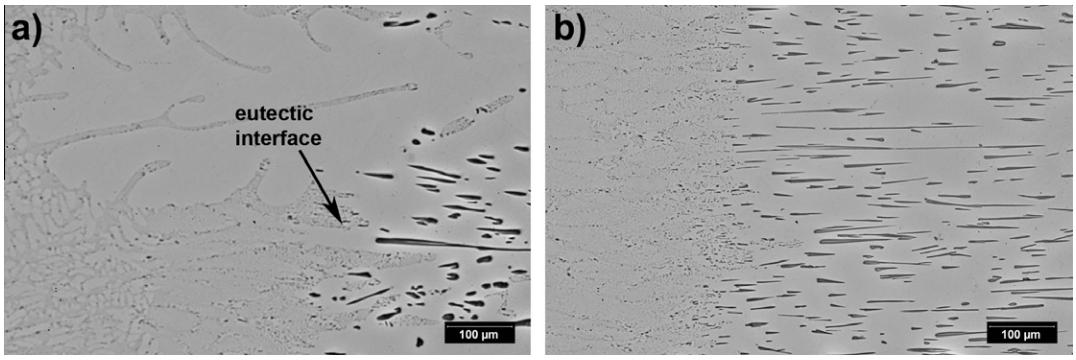

Fig. 3. Magnified views of the solid–liquid interfaces in binary eutectic specimens: (a) off-eutectic (OE) morphology in Sn–0.5 Cu grown at 10 μm s^{-1}, (b) fully eutectic (FE) morphology in Sn–0.9 Cu grown at 10 μm s^{-1}.

Table 2
Primary dendrite trunk spacing (λ_1) and freezing range (ΔT) including standard deviations.

Cu content (wt.%)	v (μm s^{-1})	λ_1 (μm)	STD (μm)	ΔT (K)	STD (K)	OE morphology
0.5	5	335	42	0.7	0.10	Dendritic
0.5	10	323	14	1.1	0.06	Dendritic
0.5	20	265	32	1.7	0.07	Dendritic
0.5	50	202	19	1.8	0.09	Dendritic
0.5	100	148	12	1.8	0.09	Dendritic
0.7	10	126	–	0.2	0.00	Cellular
0.7	20	269	13	N/A	N/A	Dendritic
0.7	50	198	15	0.5	0.06	Dendritic
0.7	100	119	15	0.5	0.08	Dendritic

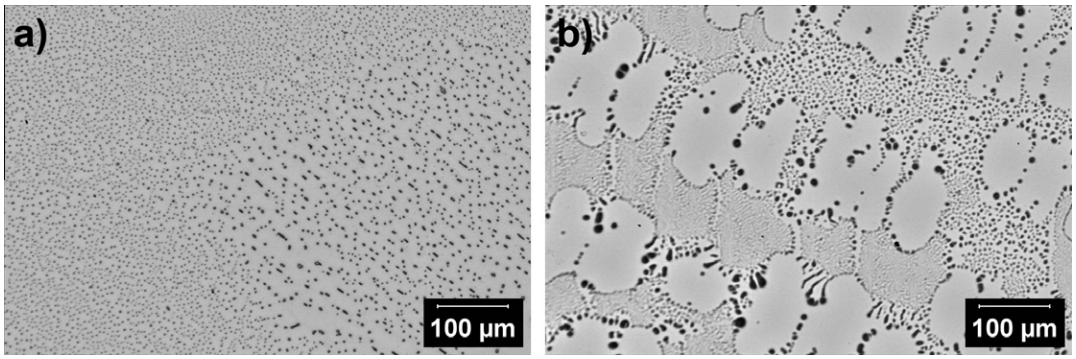

Fig. 4. (a) Optical micrograph of Sn–0.9 Cu solidified at 2 μm s^{-1} showing two domains with coarse and fine eutectic structures in a transverse cross-section. (b) Double-type eutectic structures in the interdendritic region of OE specimens (Sn–0.7 Cu specimen solidified at 20 μm s^{-1}).

As can be expected, the fraction of Cu_6Sn_5 fibres/rods increases with increasing Cu content. It appears that there is also a slight increase with increasing velocity. For all three alloys the fine eutectic microstructure has been measured as having a larger intermetallic area fraction than the coarse eutectic. For example, in the case of the Sn–0.9 Cu alloy, the fine eutectic exhibits an intermetallic area fraction of up to 7.5%, while the coarser eutectic has an area fraction of up to 4–5%. Both values are larger than the equilibrium value of 2% calculated from the phase diagram [10,11], while taking into account the density difference between Sn (7.31 g cm^{-3}) [13] and Cu_6Sn_5 (8.28 g cm^{-3}) [14].

Beyond 10 μm s^{-1}, the microstructure of Sn–0.9 Cu DS alloys changes from FE to CE, i.e., the eutectic front is no longer planar at low magnification, but develops cells as shown in Fig. 7 for various velocities. In the Sn–0.9 Cu specimen grown at 20 μm s^{-1}, two different eutectic types were observed: one with very elongated cells and the other containing ellipsoidal cells (see Fig. 7a). In the elongated cells domain, a fine layer of Sn is surrounded on one side by a coarse eutectic structure (similar to the coarse eutectic domains seen at lower speed) and with the remainder of the structure consisting of a fine eutectic (similar to the fine eutectic domains seen at lower speed) not resolved at this magnification. The transverse cell size is around 130 μm,

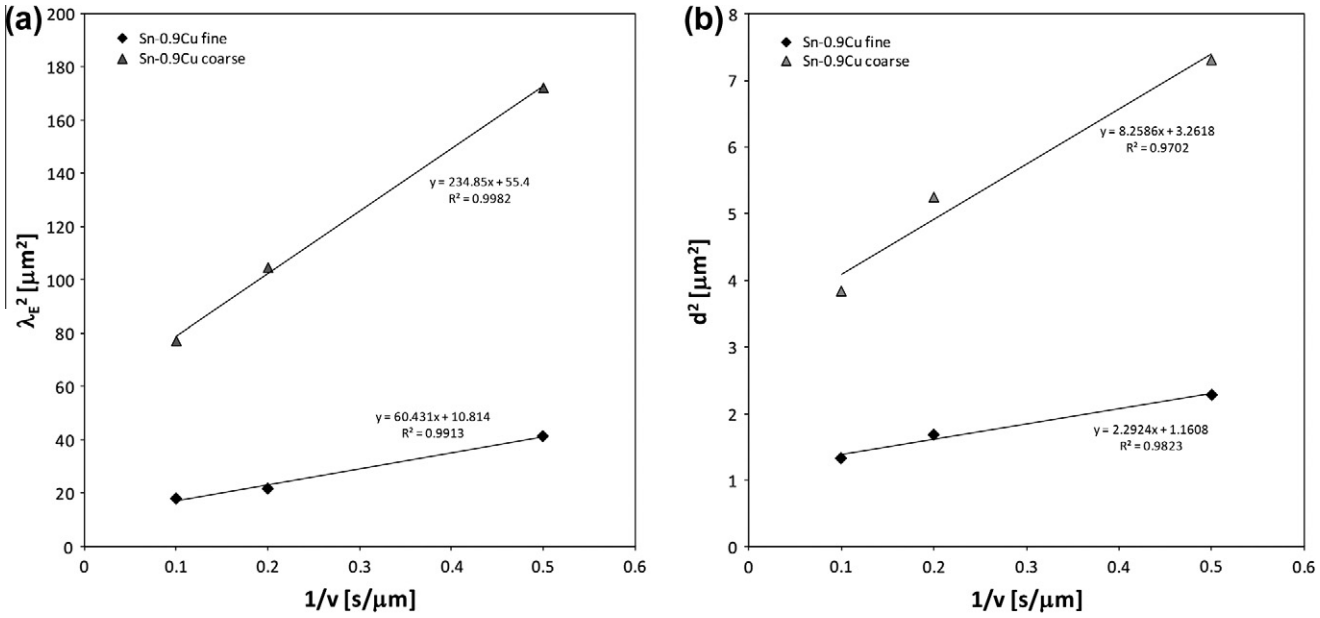

Fig. 5. (a) Square of the mean eutectic fibre spacing λ_E and (b) square of the mean fibre diameter d as a function of the inverse of the growth rate in Sn–0.9 Cu.

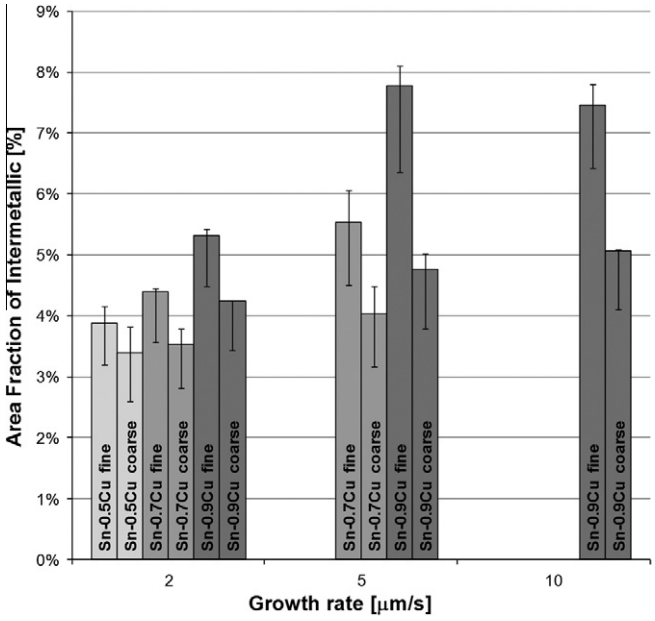

Fig. 6. Area fraction of intermetallic in FE specimens as a function of growth rate and composition. The intermetallics in the fine and coarse eutectics have been analysed separately.

which is about half the λ_1 spacing of the primary Sn phase layers measured for the two other compositions at this speed (see Table 2). For the ellipsoidal CE structure seen in Fig. 7a, the coarse eutectic is between the cells, while the fine eutectic is at the centre of the cells. At higher velocities (100 μm s^{-1}), the Sn–0.9 Cu specimen only shows the ellipsoidal CE structure (Fig. 7b). The same transformation of the eutectic into a cellular morphology is also observed for the interdendritic eutectic in Sn–0.5 Cu and Sn–0.7 Cu alloys with OE structure at velocities above 10 μm s^{-1}.

4. Discussion

The results presented in the previous section can be summarized as follows. For the lowest copper compositions, 0.5 and 0.7 wt.%, a transition from fully eutectic (FE) to off-eutectic (OE) structures is observed with increasing velocity. As the copper content increases, the velocity at which this FE–OE transition occurs increases while for the same velocity, the amount of primary β-tin dendrites/cells decreases. For the 0.9 wt.% Cu alloy, the microstructure does not show any primary phase for any of the velocities investigated (2–100 μm s^{-1}), but the structure of the eutectic evolves from FE to a cellular-type eutectic (CE). Furthermore, at low velocity, two types of eutectic domains, with coarse and fine structures, are observed. Between 10 and 20 μm s^{-1}, a transition to CE is observed, the core of the eutectic cells containing the fine eutectic while the coarse eutectic is found at intercellular regions. Similar cellular or double-type eutectic structures are also observed in the two other alloys.

The discussion is therefore structured according to the two main phenomena that are observed in the Sn–Cu specimens: first, the transition from FE to OE structures, and second, the morphology of the eutectic itself, whether found in FE or OE specimens.

The binary Sn–Cu phase relations have been of interest for a long time, especially the bronze alloys situated on the Cu-rich side. However, the various evaluations of the system still disagree on the exact composition of the eutectic point which is situated on the very Sn-rich side. There are two different eutectic compositions generally used in the literature on lead-free solders: Sn–0.9 wt.% Cu (e.g. Refs. [15,16]) and Sn–0.7 wt.% Cu. (e.g. Refs. [17–19]). The slope of the primary (Sn) liquidus is well established, while the data for the Cu_6Sn_5 liquidus scatter significantly.

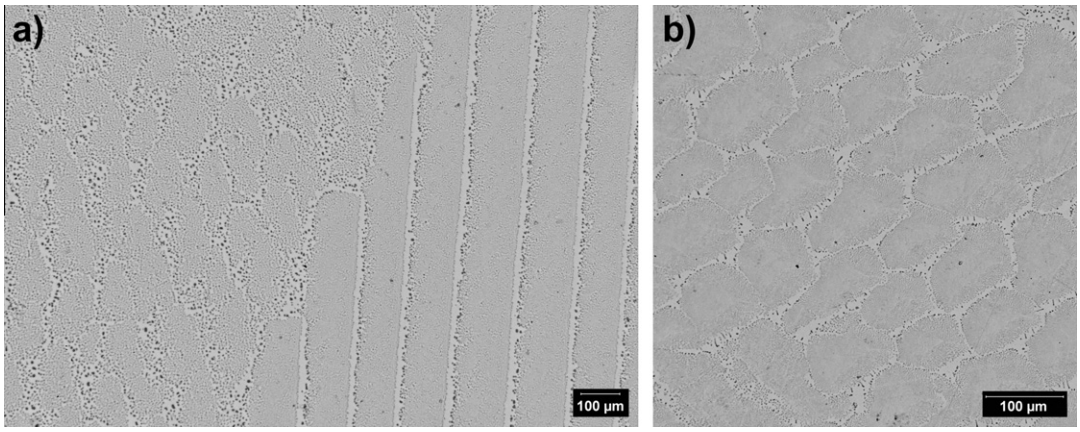

Fig. 7. Optical micrographs of transverse cross-sections of Sn–0.9 Cu specimens solidified at: (a) 20 μm s^{-1} and (b) 100 μm s^{-1} showing CE structures.

However, Moon et al. [15] showed that only 0.9 wt.% Cu is consistent with the reported eutectic temperature of 226.9 °C and the slope of the Sn liquidus. The Thermocalc® solder[1] database also uses a eutectic composition of 0.89 wt.% Cu. The observed eutectic microstructures in Sn–0.9 Cu and hypo-eutectic microstructures in Sn–0.5 Cu and Sn–0.7 Cu at intermediate cooling rates are in agreement with the phase diagram by Shim et al. [10,11], indicating that the eutectic composition is at 0.9 wt.% Cu.

The first conclusion that can be drawn from the observations summarized above is that the Sn–Cu system follows the general trend of regular eutectic alloys: for hypo-eutectic compositions, a transition from FE to OE is observed at low velocity as a result of the growth kinetics competition between the β-tin dendrites or cells and the eutectic structure [9]. Although the Cu_6Sn_5 phase is faceted [5,6], the eutectic is more or less regular with a nearly-planar eutectic front at low magnification, but still with this intermetallic phase slightly ahead of the Sn phase when looking at higher magnification. In such cases, the so-called coupled zone should not be biased too much toward the faceted phase. Therefore, the coupled zone should be fairly symmetric and the eutectic composition specimen (0.9 wt.% Cu) should not exhibit any primary β-Sn phase at any velocity. Although no higher velocity than 100 μm s^{-1} was used in this work, the actual observations confirm that only FE or CE were observed in this specimen.

Fig. 8 shows the phase diagram and a drawing of the corresponding coupled zone for near-eutectic Sn–Cu alloys. The limit between primary phase + eutectic and eutectic structure has been drawn by fitting the experimental results in this work. The coupled zone for the near-eutectic Sn–Cu alloys has previously been studied by Machida et al. [8]. Even though their experiment was carried out at a higher gradient of 4.7 K mm^{-1}, our results are in agreement with their findings. To give an impression of the complete coupled zone, the dashed line separating the eutectic structure from the primary Cu_6Sn_5 + eutectic structure has been plotted based on the results of Machida et al. [8].

For the lowest Cu content (Sn–0.5 wt.% Cu), the primary phase is clearly dendritic and arranged in layers at velocity higher than, or equal to, 5 μm s^{-1}, whereas a FE structure is observed for the lowest velocity (2 μm s^{-1}). As the copper content increases (0.7 wt.% Cu), the transition from FE to OE occurs at around 10 μm s^{-1}. These findings can be fully understood with the help of the coupled zone. According to this concept, the amount of primary phase should also increase with an increasing velocity and with decreasing copper content in hypo-eutectic alloys. Again, such is the case (compare Fig. 1a and b). What is still unclear is the structure of the primary phase itself. In the Sn–0.5 Cu and Sn–0.7 Cu

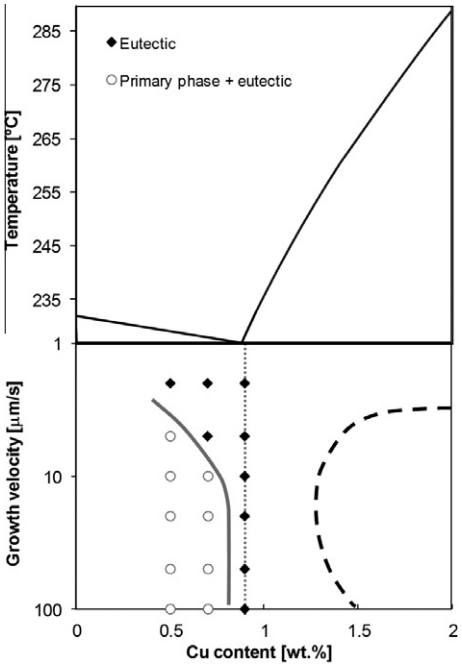

Fig. 8. Sn–Cu phase diagram showing Sn/Cu_6Sn_5 eutectic composition (calculated using Thermocalc®) and corresponding coupled zone. The region showing the stability of Cu_6Sn_5 + eutectic was plotted based on results in the literature [8].

[1] Thermocalc® NIST Solder Solutions Database USLD1, version 1.0, 1999.

specimens with dendritic structure, the primary dendrites are arranged in rows with no clear identification of primary trunks and secondary arms. It is interesting to note that while the primary spacing decreases with increasing growth rate as expected, there is no significant difference between the values for the two different Cu contents (0.5 wt.% and 0.7 wt.%) for equal velocities. β-Sn has a body-centred-cubic (bcc) tetragonal structure with a *c*-axis substantially smaller (0.3182 nm) than the *a*-axis (0.5831 nm) [20]. Unlike the statement made in Ref. [6], this high departure from cubic symmetry crystals must induce a very different growth kinetics of dendrite arms growing along [1 0 0] or [0 1 0] directions, and those growing along [0 0 1]. Considering the case of hexagonal symmetry crystals (e.g., Mg [21] or Zn [22]), it is believed that the alignment of the primary phase dendritic structure seen in Fig. 1a must be the result of [1 0 0]–[0 1 0] dendrites growing much faster than [0 0 1] dendrites. As a result, the grain selection mechanism from a random population of grains naturally gives a structure where the *c*-axis is perpendicular to the thermal gradient and the dendritic structure is aligned primarily along (0 0 1) planes. Electron backscatter diffraction (EBSD) measurements, which could not be done in the present study, should confirm this assumption.

In the Sn–0.7 Cu specimen grown at 10 μm s^{-1} (Fig. 1b), the primary phase appears as nearly symmetric isolated circles, with no particular alignment along any direction. As the liquidus of the alloy gets closer to the eutectic, the structure is probably closer to a cellular morphology, with cells barely emerging from the eutectic front as seen in the longitudinal section in Fig. 1b.

An analysis of the primary tin dendrite growth kinetics using the combined Ivantsov relationship and the marginal stability criterion with the Burden–Hunt correction was unsuccessful. This is probably because the growth kinetics of the tetragonal Sn-dendrites is not known and is also likely to be highly anisotropic. Several reasons could explain this observation. First of all, all dendrite models are based on regularly distributed dendrites. The dendrites in the Sn–Cu near-eutectic alloys grow in rows with no clear identification of primary trunks and secondary arms. Secondly, the Ivantsov relationship has been developed for a parabolic dendrite tip, which is probably not applicable for β-Sn with its tetragonal crystal structure. A phase field model could probably be used, but in that case the anisotropy of the solid–liquid interfacial energy would be required.

Even though it is not possible to calculate the growth kinetics of the eutectic phase, the results for the freezing range ΔT measured for all composition-velocity couples leading to dendritic structure (see Table 2) show that the solidification range first increases and then stabilizes for increasing growth velocities for both hypo-eutectic alloys. For both alloys the measured values for the freezing range ΔT are lower than ΔT_0 (the equilibrium solidification range determined based on the phase diagram), most probably due to the fact that the β-Sn dendrites grow at a larger undercooling than the Sn/Cu_6Sn_5 eutectic.

As previously reported by Drevet et al. [5,6], two eutectic morphologies are present in the specimens. At low speed, the coarse and fine eutectics appear as separate domains, or grains. For both of them, Drevet et al. identified that the Cu_6Sn_5 fibres grow with the basal plane of its hexagonal structure perpendicular to the thermal gradient (or parallel to the eutectic front) by transmission electron microscopy (TEM). They attributed the two morphologies to a difference in interfacial energies, but the mechanism remains unclear. Since EBSD was not done, it could indeed be due to two different orientations of the β-Sn phase, e.g., with the *a*- or *c*-axis growing parallel to the thermal gradient. It could be also due to trace elements present in the alloys, even though Drevet et al. used much higher-purity tin and copper components.

The two types of eutectic (coarse and fine) were observed in all the specimens, but their distribution within the eutectic regions changed with the velocity, and to some extent with composition. In the Sn–0.9 Cu alloy, where no primary tin phase was observed across the whole velocity range from 2 to 100 μm s^{-1}, the two eutectics appear as isolated domains at low speed and as cells for higher velocity. In the cells, whether elongated or ellipsoidal, the fine eutectic is always at the centre of the cell and the coarse eutectic is at the periphery. The same isolated domains with two different types of eutectic, as well as the cells at higher velocities, were also observed in the Sn–0.5 Cu and Sn–0.7 Cu specimens with OE structures. Drevet et al. [6] studied the eutectic Sn–0.9 Cu and also observed the co-existence of two grains of different microstructure in terms of mean eutectic fibre spacing λ_E and fibre size over the whole length of sample. Drevet et al. [6] observed a large λ_E which is two to three times greater than the small λ_E which is very similar to that observed in the present work where the λ_E for the coarse eutectic is twice that of the fine eutectic.

The results for the area fraction of intermetallics in Fig. 6 indicate that the amount of intermetallic phase decreases with decreasing Cu content, in agreement with a more hypo-eutectic structure. However, the solid fractions of intermetallic measured in the eutectic Sn–0.9 Cu alloys (see Fig. 6) is much higher than the value of ~2 vol.% expected based on the equilibrium phase diagram, with an average of 5.8 vol.% Cu_6Sn_5 in the eutectic Sn–0.9 Cu alloy. There are several potential causes for this discrepancy. First of all, the phase diagram is valid for alloys solidified at equilibrium conditions which may not be the case for these samples. It has also been observed above in the analysis of the dendritic growth that the β-Sn dendrites grow at a larger undercooling than the Sn/Cu_6Sn_5 eutectic, which may lead to preferential growth of the intermetallic phase. Finally it is also important to note that the fibres are not very regularly distributed and that it is therefore difficult to obtain measurements representative for the whole sample.

Drevet et al. [5,6] did not observe a cellular eutectic structure in their work which was done at similar growth rates as the present study, but using higher-purity tin and copper components. We therefore attribute the transition

from FE to CE in the Sn–0.9 Cu specimen to a destabilization of the eutectic front due to segregation of a third solute impurity. As the eutectic interface consists of more than 97% of Sn, it is sufficient for the analysis to consider the rejection of a third trace element by a tin front, neglecting the possible rejection (or absorption) of the same element by the Cu_6Sn_5 intermetallic. In the chemical analysis of our alloys (see Table 1), the major trace impurities are Pb (350 ppm) and Sb (200 ppm). Since the peritectic phase Sn–Sb phase diagram shows a partition coefficient close to unity (1.1), we only consider the partitioning of the lead impurities.

Constitutional undercooling of a Sn–0.035 wt.% Pb planar front occurs at a velocity v_{crit} given by:

$$v_{crit} = \frac{GD_\ell}{\Delta T_0} \quad (1)$$

where $\Delta T_0 = m_\ell C_0(k_0 - 1)/k_0$ is the solidification interval of the alloy, m_ℓ is the slope of the liquidus, C_0 is the nominal composition, k_0 the partition coefficient of Pb, G is the thermal gradient and D_ℓ is the diffusion coefficient of Pb in the liquid. Taking values from the phase diagram for k_0 and m_ℓ ($k_0 = 0.063$ and $m_\ell = -1.28$ K/wt.%) and from Refs. [23,24] for the diffusion coefficient ($D_\ell = 3.7 \times 10^{-9}$ [24] and 7.8×10^{-9} m^2 s^{-1} [23]), the destabilization of a tin front by 350 ppm Pb in a gradient of 2500 K m^{-1} occurs at 13.8 and 23.1 μm s^{-1}, respectively. This value is in very good agreement with the change from FE to CE observed between 10 and 20 μm s^{-1} in the Sn–0.9 wt.% Cu specimen. Thus we conclude that this eutectic morphology transition is due to the Pb impurities in the alloys and that only 350 ppm Pb is sufficient to significantly change the microstructure in these alloys.

If the influence of Pb on the transition from FE to CE is confirmed, several questions nevertheless remain concerning the reason for observing the co-existence of two types of eutectics, i.e. coarse and fine. Even though Drevet et al. [5,6] used very-high-purity base elements, could this be due to trace elements such as lead? Does the fine eutectic correspond to the pure binary Sn–Cu system, while trace elements such as Pb are segregated during growth and give a coarser eutectic? Does the coarse structure occur due to a change of the interfacial energy induced by these trace elements or by various orientations of the tin phase? Further work is needed, in particular EBSD work to study the alignment of the tin phase, but also TEM diffraction to study the crystallographic properties of the intermetallics present in the two types of eutectics. Furthermore, the influence of Ni additions and therefore the effects of solidification kinetics on microstructure formation in ternary Sn–Cu–Ni solder alloys are of future interest.

5. Conclusions

This study focuses on the microstructure formation in near-eutectic Sn–Cu solder alloys during directional solidification at different cooling rates. Three main phenomena have been observed in these alloys: First, the transition from a fully eutectic to an off-eutectic microstructure with increasing growth rate, due to a coupled zone. Although Cu_6Sn_5 is a faceted phase, the eutectic is weakly irregular and consequently the coupled zone is fairly symmetric. Second, a transition from fully eutectic to cellular eutectic structures occurs as the growth rate is increased. It has been shown that this morphology change is most probably due to segregation of trace impurities, more specifically Pb. And, finally, the coexistence of two eutectic grains, one with a very fine fibre spacing and the other with a much coarser morphology and larger spacing, have been identified and confirm the previous results of Drevet et al. Further work is required to explain the origin of this phenomenon.

Acknowledgements

The authors would like to thank Nihon Superior Co. Ltd., Japan, for providing the alloys and for conducting the chemical analysis. One of the authors (TV) gratefully acknowledges the financial support provided by the University of Queensland Research Scholarship (UQRS), the UQ School of Engineering Scholarship as well as Nihon Superior Co. Ltd., Japan.

References

[1] Directive 2002/95/EC of the European Parliament and of the Council of 27 January 2003 on the restriction of the use of certain hazardous substances in electrical and electronic equipment. <http://europa.eu.int/eur-lex/pri/en/oj/dat/2003/l_037/l_03720030213en00190023.pdf>.
[2] Bradley E, Handwerker CA, et al. Lead-free electronics. Chichester: John Wiley & Sons; 2007.
[3] Nishimura T. In: International patent EP1043112; 1999.
[4] Nishimura T, Suenaga S, Ikeda M. In: PRICM4; 2001.
[5] Drevet B, Garandet JP, et al. J Cryst Growth 1993;129:549–58.
[6] Drevet B, Camel D, et al. Acta Mater 1996;44(10):4071–84.
[7] Grugel RN, Brush LN. Mater Character 1997;38:211–6.
[8] Machida J, Esaka H, et al. J Jpn Inst Metals 2006;70(1):73–9.
[9] Kurz W, Fisher DJ. Int Metals Rev 1979;5 and 6:177–204.
[10] Shim JH, Oh CS, et al. Z Metallkd 1996;87(3):205–12.
[11] NIST, Cu–Sn System. In: Phase diagrams and computational thermodynamics; 2003. <http://www.metallurgy.nist.gov/phase/solder/cusn.html>.
[12] Gourlay CM, Yamamoto Y, et al. submitted for publication.
[13] Davis JR, editor. Metals handbook materials park. OH: ASM International; 1998.
[14] Fields RJ, Low SR. Physical and mechanical properties of intermetallic compounds commonly found in solder joints. <http://www.metallurgy.nist.gov/mechanical_properties/solder_paper.html>.
[15] Moon K-W, Boettinger WJ, et al. J Electron Mater 2000;29(10):1122–36.
[16] Kattner UR. JOM 2002;54(12):45–51.
[17] Abtew M, Selvaduray G. Mater Sci Eng R 2000;27(5–6):95–141.
[18] Suganuma K. Curr Opin Solid State Mater Sci 2001;5(1):55–64.
[19] Lin C-H, Chen S-W, Wang C-h. J Electron Mater 2002;31(9):907–15.
[20] Wolcyrz M, Kubiak R, Maciejewski S. Phys Status Solidi B 1981;107(1):245–53.
[21] Pettersen K, Ryum N. Metall Trans A 1989;20(5):847–52.
[22] Rheme M, Gonzales F, Rappaz M. Scripta Mater 2008;59(4):440–3.
[23] Klassen M, Cahoon J. Metall Mater Trans A 2000;31(5):1343–52.
[24] Lide DR. Handbook of chemistry and physics. 71st ed. Boca Raton (FL): CRC Press; 1990.